Analysis of Flexural Behavior and Lateral Buckling of Inelastic Steel Beams under Cyclic Loads

AUTHOR(S):

GOTO, Hisao; KAMEDA, Hiroyuki; KODAMA, Yutaka

CITATION:

GOTO, Hisao ...[et al]. Analysis of Flexural Behavior and Lateral Buckling of Inelastic Steel Beams under Cyclic Loads. Memoirs of the Faculty of Engineering, Kyoto University 1978, 39(4): 446-481

ISSUE DATE:

1978-01-31

URL:

http://hdl.handle.net/2433/281049

Analysis of Flexural Behavior and Lateral Buckling of Inelastic Steel Beams under Cyclic Loads

By

Hisao GOTO,* Hiroyuki KAMEDA,* and Yutaka KODAMA**

(Received June 17, 1977)

Abstract

Inelastic steel beams are analyzed with emphasis on their transient flexural behavior and lateral buckling under cyclic loads. The constraint and load conditions are chosen so that they simulate inelastic beams of a frame structure subjected to a horizontal seismic motion.

An analytical model of inelastic beams is proposed that accounts for basic transient behaviors of mild steel. On this basis, a detailed discussion is made on the mechanism of transient behaviors including those of the plasic hinge, load-deflection relation, lateral buckling load, etc. A physical interpretation is given as regards the transient flexural behavior and the deformation capacity for the lateral buckling of steel beams under monotonic and cyclic loadings.

1. Introduction

In a structural design for severe seismic loads, the post yielding deformation capacity of structures and structural elements is of great importance. It has been recognized that the mechanism of absorbing dynamic energy imparted to structures during strong earthquakes primarily relies upon the hysteretic energy dissipation by structural elements. Such an energy dissipation capacity has become at least implicitly a basic requirement in the design philosophy of modern structures to withstand seismic loads.

To provide an adequate energy dissipation capacity, the structure must possess stable elastoplastic force-deflection properties under cyclic loads. Structural steel is an excellent material to meet this requirement. Because of its great ductility and stable hysteresis loops under repeated large deformations, structural steel is considered

* Department of Transportation Engineering.
** Pacific Consultants Co., Ltd.

as one of the most reliable structural materials for earthquake resistant designs.

Unstable hysteretic behavior of steel structures occurs more for structural reasons than being caused by material properties. The desired hysteretic capacity may be violated through the gravity effect on columns and the lateral buckling of beams. Such instability, including lateral buckling of beams under cyclic loads, has been studied experimentally by several authors[2),6),8),11)]. All of them arrived at a similar conclusion, namely that once lateral buckling takes place in a steel beam the hysteresis curves can no longer withstand further load reversals, and furthermore the resistance of the beam is reduced successively under repeated deformation with a constant amplitude. It was also pointed out that the deformation capacity of flexural beams for lateral buckling is much smaller for cyclic deformation than would be expected from monotonic loading.

Tanaka, Takanashi, and Udagawa[8)], and Takanashi[6)] obtained the rotation capacity for cyclic and monotonic loadings for beams with various slenderness ratios. Goto, Kameda, Koike, et. al.[2)] made a detailed discussion of the time dependent behavior of steel beams under cyclic loads, with and without lateral buckling. It was pointed out that the number of load cycles up to lateral buckling depends on the amplitude of cyclic deformation, implying a step-by-step effect of strain hardening. Time variation of stiffness and hysteretic energy per cycle, and total hysteretic energy capacity were also discussed.

Thus the typical behavior of lateral buckling of steel beams under cyclic loads may be summarized as a low deformation capacity compared to monotonic loading, and a possible effect of step-by-step strain hardening on initiation of buckling. This implies the importance of the transient behavior of inelastic beams. Most of the earlier studies on the cyclic behavior of inelastic beams were focused primarily on their steady state, and analytical models have been proposed also for steady-state hysteresis loops. Precise discussion of the transient flexural process is required as to the properties of plastic hinges and the variation of tangent rigidities as well as conventional load-deformation relations.

The objective of this study is to provide a physical basis for a rational interpretation of the foregoing experimental results, using an analytical model of elastoplastic beams. First, steel beams are modeled with laminated elements having an elastoplastic stress-strain relation with a strain-hardening effect. Then, the transient post yielding flexural behavior of the model is analyzed for monotonic and cyclic loadings with primary attention given to the behavior of the mid-span plastic hinge. In the analysis of inelastic lateral buckling, the results for the flexural behavior are combined with the strain-energy method using the tangent rigidities. On the basis of these results, a physical interpretation is presented in regard to the difference in the

deformation capacity of inelastic steel beams for monotonic and cyclic deformation. This study should provide useful information for establishing design criteria for steel beams subjected to a strong seismic load.

2. Analytical Model

2.1. Load conditions

The analytical model dealt with herein is intended to explain behaviors of tested steel beams whose loading and support conditions are such as those illustrated in Fig. 1(a). For the strong axis, they constitute simply supported beams subjected to a cyclic deformation at mid-span. The plastic region is concentrated in the mid-span

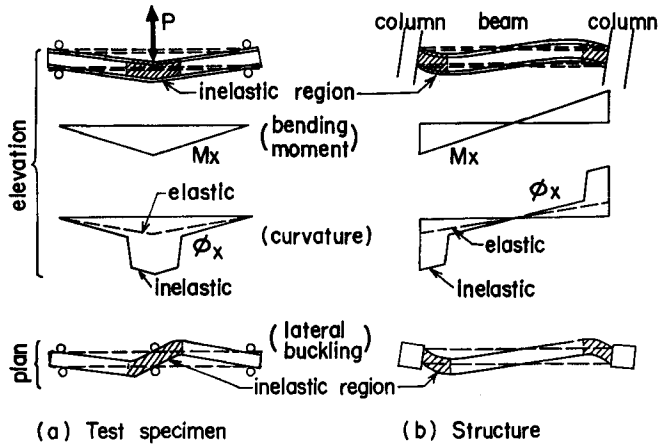

Fig. 1. Constraint Conditions of Steel Beams; Test-Structure Analogy.

region as shown in this figure, which also illustrates the distribution of the bending moment and the curvature for elastic and inelastic states. For the weak axis, these steel beams are double span continuous beams. They may undergo lateral buckling of the second mode. The conditions described above were realized in the test procedures[2),8)] which results are compared with the analytical results in this study. Such test conditions will be an analogy to steel beams in practical structures with strong columns which are subjected to large deformation in response to earthquake excitation. Such a situation is illustrated schematically in Fig. 1(b). Half length of the practical beams may be realized in that of the tested beams.

2.2. Geometrical conditions

Size parameters and location parameters of the steel beams analyzed herein are shown in Fig. 2. The beam is subjected to a cyclic load P acting at $z=0$ in $y-$ direction. The displacement of the shear center of a beam section is illustrated in

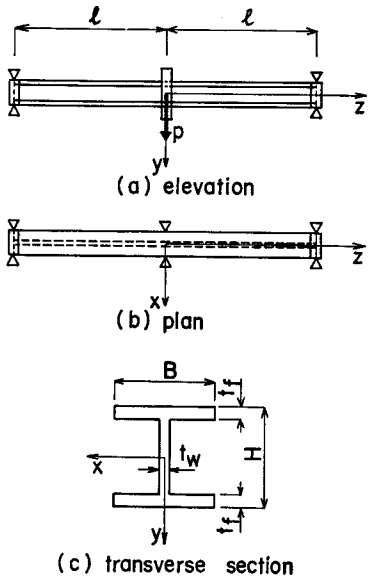

Fig. 2. Tested Beams.

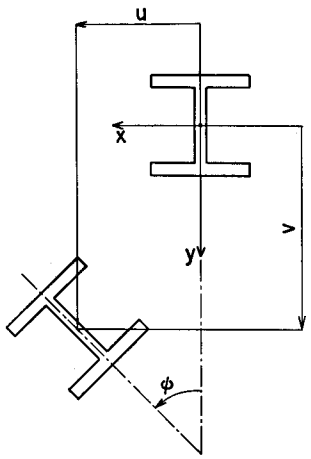

Fig. 3. Description of Beam Deformation.

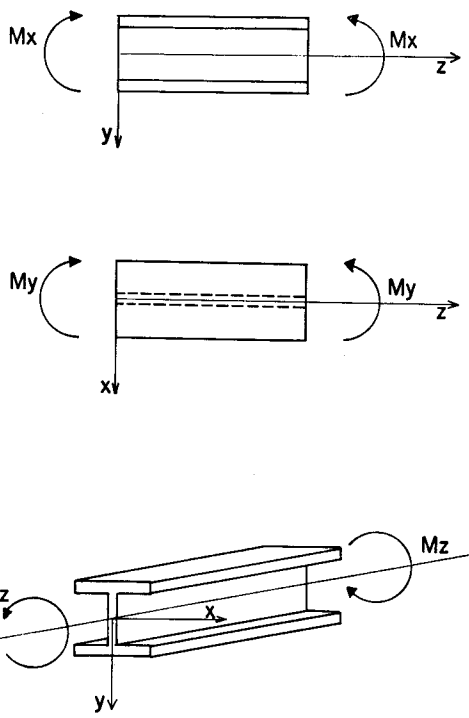

Fig. 4. Description of Moments.

Fig. 3. The vertical displacement v arises from the cyclic load P, and the horizontal displacement u and rotation ϕ are induced by lateral buckling.

The boundary conditions consistent with the constraints shown in Fig. 2 are as follows.

Constraints on flexure:

$$\left.\begin{aligned} &z=\pm l; \quad v=0 \text{ and } \frac{d^2v}{dz^2}=0 \\ &z=0; \quad \frac{dv}{dz}=0 \end{aligned}\right\} \qquad \cdots\cdots\cdots(1)$$

Constraints on lateral buckling:

$$z=\pm l \text{ and } 0; \quad u=0, \ \frac{d^2u}{dz^2}=0, \ \phi=0 \text{ and } \frac{d^2\phi}{dz^2}=0 \qquad \cdots\cdots\cdots(2)$$

Positive directions of the bending moment and the torque are shown in Fig. 4.

2.3. Stress-strain relations

The analytical model for the stress-strain relation used in this study is shown in Fig. 5. It accounts for the typical inelastic cyclic behaviors of mild steel which have been demonstrated through laboratory tests[1),7),12)], including the vanishing of the yield zone and a successive hardening by repeated cyclic loading. In Fig. 5, the path O→A→B→C in the initial loading undergoes the yield zone at the constant yield stress σ_Y which is followed by the strain hardening. The unloading path C→D is elastic until the stress reaches $-\sigma_Y$, and the strain hardening starts immediately after D. Further stress reversals result in the path E→F→G and so on without a constant-stress yield zone in any further hysteresis loops. Since the yield points are fixed at $\pm\sigma_Y$, the peak stress increases with increasing strain amplitude. This is the general behavior observed in experimental data[1)]. The specific value of the yield level $\pm\sigma_Y$, except the initial yielding, has no physical significance: it is for the sake of bilinear modeling. Actual hysteretic paths are smoother lines such as shown by the dashed line in Fig. 5 because of the Bauschinger effect.

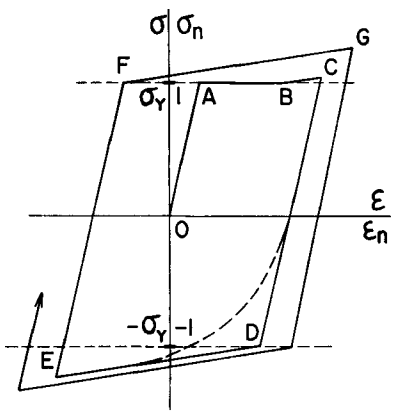

Fig. 5. Stress-Strain Relation Model.

To determine the parameter values for the stress-strain relation described above,

ten test specimens (No. 7 standard) were cut out from the flanges of an SS41 H-sectioned (100×100×6×8 mm) steel bar, and were tested in monotonic tensile stress. A typical test result is shown in Fig. 6. The required values obtained from these test results are as follows:

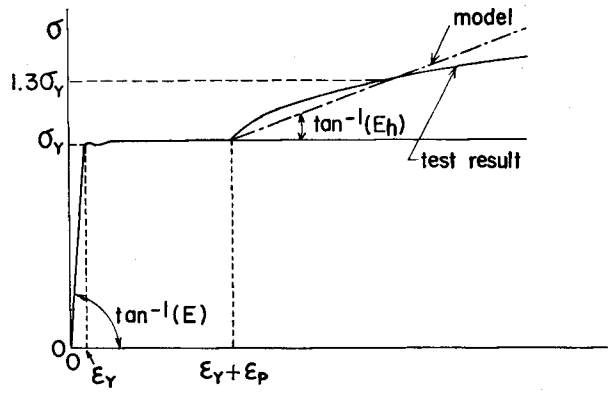

Fig. 6. Typical Stress-Strain Curve.

yield stress; $\sigma_Y=2\ 799\ \mathrm{kg/cm^2}$
yield strain; $\varepsilon_Y=0.1429\ \%$
elasitc modulus; $E=\sigma_Y/\varepsilon_Y=1.959\times10^6\ \mathrm{kg/cm^2}$
strain range of yield zone; $\varepsilon_p=1.77\ \%$
strain hardening modulus; $E_h=3.119\times10^4\ \mathrm{kg/cm^2}$
strain hardening factor; $h=E/E_h=62.8$

Using the above notaitons, the relation between the stress increment $\Delta\sigma$ and the strain increment $\Delta\varepsilon$ is given by

$$\Delta\sigma=E'\,\Delta\varepsilon \qquad \cdots\cdots(3)$$

in which

$$E'=\begin{cases}E & : \text{elastic region}\\ 0 & : \text{yield zone}\\ E_h=E/h & : \text{strain-hardening region}\end{cases} \qquad \cdots\cdots(4)$$

In the subsequent analysis, the following non-dimensional notations are used.

$$\begin{aligned}&\sigma_n=\sigma/\sigma_Y\\ &\varepsilon_n=\varepsilon/\varepsilon_Y\\ &\varepsilon_{pn}=\varepsilon_p/\varepsilon_Y=11.4\end{aligned} \qquad \cdots\cdots(5)$$

for which Eq. (3) yields

$$\Delta\sigma_n = e\Delta\varepsilon_n \qquad \cdots\cdots(6)$$

where

$$\left.\begin{aligned}\Delta\sigma_n &= \Delta\sigma/\sigma_Y\\ \Delta\varepsilon_n &= \Delta\varepsilon/\varepsilon_Y\\ e &= E'/E\end{aligned}\right\} \qquad \cdots\cdots(7)$$

Stress amplitude σ_a for a steady state hysteresis loop with a strain amplitude of ε_a is represented by

$$\sigma_a = \begin{cases}\varepsilon_a; & 0 \leqq \varepsilon_a \leqq 1\\ \dfrac{2}{h+1}\varepsilon_a + \dfrac{h-1}{h+1}; & \varepsilon_a \geqq 1\end{cases} \qquad \cdots\cdots(8)$$

Eq. (8) also gives the "skeleton curve" connecting the peaks of hysteresis loops. Tanabashi et. al.[7] represented the skeleton curve for the tension-compression test on SS41 steel specimens by the Ramberg-Osgood model given by

$$\varepsilon_a = r_s^{1-\bar{n}}\,\sigma_a\,|\sigma_a|^{\bar{n}-1} \qquad \cdots\cdots(9)$$

with $r_s=0.644$, and $\bar{n}=3.8$. Eq. (8) and (9) are compared in Fig. 7 for $h=62.8$. Agreement between the two formulas is satisfactory in the practical range.

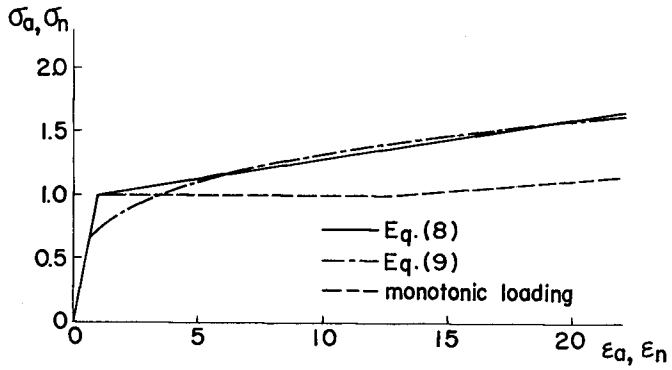

Fig. 7. Relation between Stress Amplitude and Strain Amplitude.

In addition to the above properties related to the normal stress and strain the shear modulus G is assumed to have the following value.

$$G = 8.1\times10^5\ \mathrm{kg/cm^2}$$

2.4. Basic assumptions for analysis

The inelastic cyclic behavior of steel beams as modeled previously is analyzed in the subsequent chapters. The analysis is made under the following assumptions:

(i) Each transverse section of the beam which was initially plane remains plane and normal to longitudinal fibers, and its initial shape is preserved after deformation.

(ii) The yield condition of the beam and the plastic deformation thereof are determined by longitudinal bending stress.

(iii) The whole area of the transverse section is effective with constant shear modulus in evaluating the torsional rigidity.

(iv) Effect of shear on transverse deformation is negligible.

(v) Effects of initial residual stress and local flange buckling are negligible.

(vi) There is no initial deformation nor eccentric load.

(vii) Lateral buckling is analyzed by using the tangent modulus theory. For this purpose, two cases are considered for the tangent modulus in evaluating the weak-axis flexural rigidity and the warping rigidity: if ε'_{pn} denotes the strain range of the yield zone for calculating the above two rigidities, (a) $\varepsilon'_{pn}=\varepsilon_{pn}$, ε_{pn} being given in Eq. (5), or (b) $\varepsilon'_{pn}=0$.

These assumptions are simpler than a more detailed analysis based on yield conditions including the effect of shear, change in the sectional shape under tension and compression, and those initial and local irregularities neglected by the assumptions (v) and (vi). However, they may be justifiable as a first-order approximation for H-beams under the constraint conditions in Fig. 1 whose inelastic behavior is dominated by flanges, and also for the inelastic cyclic load for which detailed information on the effect of initial and local irregularities depends on future studies. This allows one to assume that the beams are symmetrical about the xz-plane, and that the neutral axis and the shear center coincide with the centroid of the transverse section.

The two cases considered in the assumption (vii) would correspond to two extreme cases. Case (a) to assert $\varepsilon'_{pn}=\varepsilon_{pn}$ is consistent with Eq. (4) developed for the analysis of a strong-axis flexural behavior in the plane containing the external load P. This assumption results in almost a complete loss of lateral rigidity immediately after the first yielding, and a very low deformation capacity against lateral buckling is obtained. However, excessive lateral buckling usually does not develop at the initial flange yielding. Excessive lateral buckling usually occurs when the beam is in the strain-hardening region.[2] The critical load for lateral buckling in the strain hardening region is obtained from case (b) of assumption (vii) which ignores the yield zone in calculating lateral rigidities by setting $\varepsilon'_{pn}=0$.

These arguments may be justified if the behavior of the yield zone as described by Lay[5] is considered. He emphasized that the yield zone is only an apparent macroscopic behavior. Actually, only unstable slips can occur instantaneously at

discrete sections along the length of the beam. Then it follows that lateral buckling caused by a loss of rigidity in the yield zone can result only in a limited lateral deflection, whereas the yield zone contributes fully to the accumulation of deflection in the direction of the load P.

2.5. Curvature, moment, and section rigidities

Based on the assumptions described in the foregoing sections, the bending-moment-curvature relation and the section rigidities can be obtained. The section rigidities herein denote those based on the tangent modulus at each state, including the flexural rigidity about the strong axis EI_x, that for the weak axis EI_y, warping rigidity EI_w, and torsional rigidity GJ. These rigidities for the elastic region are represented by[9]

$$\left.\begin{aligned}(EI_x)_E &= \frac{E}{12}\{B H^3-(B-t_w)(H-2t_f)^3\}\\ (EI_y)_E &= \frac{E}{12}\{2B^3 t_f+(H-2t_f)\,t_w^3\}\\ (EI_w)_E &= \frac{E}{24}(H-t_f)^2 t_f B^3\\ (GJ)_E &= \frac{G}{3}\{2B t_f^3+(H-t_f)\,t_w^3\}\end{aligned}\right\} \quad \cdots\cdots\cdots (10)$$

in which $(\ )_E$ stands for the elastic rigidity.

For a nondimensional representation, the coordinate system in Fig. 2 is normalized as

$$\left.\begin{aligned}x_n &= x/r_y\\ y_n &= y/r_x\\ z_n &= z/l\end{aligned}\right\} \quad \cdots\cdots\cdots (11)$$

in which x_n, y_n, z_n=non-dimensional coordinates, and r_x, r_y=radii of gyration about x- and y-axes, respectively, given by

$$\left.\begin{aligned}r_x &= \sqrt{(EI_x)_E/EA_0}\\ r_y &= \sqrt{(EI_y)_E/EA_0}\end{aligned}\right\} \quad \cdots\cdots\cdots (12)$$

where A_0 is the sectional area of the beam given by

$$A_0 = 2t_f B + t_w (H-2t_f) \quad \cdots\cdots\cdots (13)$$

In the analysis of lateral buckling in a later chapter, the slenderness ratio about the weak axis given as follows is one of the principal ruling parameters:

$$\lambda = \frac{l}{r_y} \quad \cdots\cdots\cdots (14)$$

The normalized curvatures ϕ_{xn}, ϕ_{yn} of the beam about the x- and y-axes, respectively, are represented by

$$\left.\begin{aligned}\phi_{xn}&=\phi_x/\phi_{xY}\\ \phi_{yn}&=\left(\frac{r_y}{r_x}\right)^2\frac{\phi_y}{\phi_{xY}}\end{aligned}\right\} \qquad \cdots\cdots(15)$$

in which ϕ_x, ϕ_y=the curvature about the x- and y-ayes, and $\phi_{xY}=2\varepsilon_Y/H$=the value of ϕ_x at the initial fiber yielding.

The bending moments M_x and M_y are also represented in the following nondimensional form:

$$\left.\begin{aligned}M_{xn}&=\frac{M_x}{M_{xY}}\\ M_{yn}&=\frac{M_y}{M_{xY}}\end{aligned}\right\} \qquad \cdots\cdots(16)$$

where M_{xY} is the yield bending moment about the x-axis given by

$$M_{xY}=\frac{2r_x^2A_0}{H}\sigma_Y \qquad \cdots\cdots(17)$$

The non-dimensional bending moment M_{xn} is generally represented by

$$M_{xn}=\frac{1}{M_{xY}}\int_A\sigma\, y\, dA=\frac{H}{2r_x}\int_{A_n}\sigma_n\, y_n\, dA_n \qquad \cdots\cdots(18)$$

where A_n is the normalized area given by

$$A_n=\frac{A}{A_0} \qquad \cdots\cdots(19)$$

Since the relation between the normalized strain ε_n in Eq. (5) and the normalized curvature in Eq. (15) is given by

$$\varepsilon_n=\frac{y\,\phi_x}{\varepsilon_Y}=\frac{2r_x}{H}y_n\,\phi_{xn} \qquad \cdots\cdots(20)$$

Eq. (6) yields

$$\Delta\sigma_n=\frac{2r_x}{H}e\,y_n\,\Delta\phi_{xn} \qquad \cdots\cdots(21)$$

Hence, the non-dimensional bending moment increment ΔM_{xn} about the x-axis is given by

$$\Delta M_{xn}=\frac{H}{2r_x}\int_{A_n}\Delta\sigma_n\, y_n\, dA_n=\left[\int_{A_n}e\,y_n^2\, dA_n\right]\Delta\phi_{xn} \qquad \cdots\cdots(22)$$

Likewise, the non-dimensional bending moment increment ΔM_{yn} about the y-axis is

obtained as

$$\Delta M_{yn}=\left[\int_{A_n} e\,x_n^2\,dA_n\right]\Delta\phi_{yn} \qquad \cdots\cdots(23)$$

Eqs. (22) and (23) can be rewritten as

$$\left.\begin{aligned}\Delta M_{xn}&=(EI_x)_n\,\Delta\phi_{xn}\\ \Delta M_{yn}&=(EI_y)_n\,\Delta\phi_{yn}\end{aligned}\right\} \qquad \cdots\cdots(24)$$

in which $(EI_x)_n$ and $(EI_y)_n$ are non-dimensional tangent flexural rigidities represented by

$$\left.\begin{aligned}(EI_x)_n&=\int_{A_n} e\,y_n^2\,dA_n\\ (EI_y)_n&=\int_{A_n} e\,x_n^2\,dA_n\end{aligned}\right\} \qquad \cdots\cdots(25)$$

Next, the tangent warping rigidity $(EI_w)_T$ is considered. Let $(EI_f)_T$ denote the tangent flexural rigidity of a single flange about the y-axis. Then, since biaxially symmetric cross sections are being discussed, the warping rigidity $(EI_w)_T$ is given by[9]

$$\begin{aligned}(EI_w)_T&=\frac{1}{2}(H-t_f)^2\,(EI_f)_T=\frac{1}{2}(H-t_f)^2\int_{A_f} E'\,x^2\,dA\\ &=\frac{1}{2}(H-t_f)^2\,E\,r_y^2\,A_0\int_{A_{fn}} e\,x_n^2\,dA_n=\frac{1}{2}(H-t_f)^2\,(EI_y)_B\int_{A_{fn}} e\,x_n^2\,dA_n\end{aligned} \qquad \cdots\cdots(26)$$

The non-dimensional tangent warping rigidity is given by

$$(EI_w)_n=\frac{(EI_w)_T}{(EI_w)_B}=\left\{2+\frac{(H-t_f)\,t_w^3}{B^3\,t_f}\right\}\int_{A_{fn}} e\,x_n^2\,dA_n \qquad \cdots\cdots(27)$$

Since it is assumed that the tangent shear modulus is constant, and the whole sectional area is always effective in evaluating the torsional rigidity, the non-dimensional torsional rigidity $(GJ)_n$ becomes

$$(GJ)_n=\frac{(GJ)_T}{(GJ)_B}\equiv 1 \qquad \cdots\cdots(28)$$

3. Flexural Behavior of Elastoplastic Beams

3.1. Description of load and deflection

The inelastic beams dealt with herein are simple beams in the $y-z$ plane with the cyclic load P applied at midspan in the y-direction as shown in Fig. 2. If P_Y denotes the yield load at the initial yielding of the flange, and δ_Y denotes the corresponding midspan displacement, we have

$$P_Y=\frac{2M_{xY}}{l}=4E\varepsilon_Y A_0\frac{r_x^2}{lH} \quad \cdots\cdots (29)$$

$$\delta_Y=\frac{P_Y l^3}{6(EI_x)_E}=\frac{1}{3}\phi_{xY} l^2 \quad \cdots\cdots (30)$$

In the following, the load P and the displacement v of an arbitrary section in the y-direction are represented by the corresponding non-dimensional terms P_n and v_n, respectively, given by

$$P_n=P/P_Y \quad \cdots\cdots (31)$$

$$v_n=v/v_Y \quad \cdots\cdots (32)$$

Accordingly, the non-dimensional midspan displacement is given by

$$\delta_n=v_n|_{z_n=0} \quad \cdots\cdots (33)$$

By using these notations, the bending moment M_{xn} is represented by

$$M_{xn}=(1-|z_n|)P_n \quad \cdots\cdots (34)$$

By virtue of the well-known curvature-displacement relation and Eqs. (11), (15), (30) and (32), the non-dimensional curvature ϕ_{xn} takes the form

$$\phi_{xn}=-\frac{1}{3}\frac{d^2v_n}{dz_n^2} \quad \cdots\cdots (35)$$

In Eq. (35), the effect of the slope dv_n/dz_n is neglected since its effect is of the order of 10^{-2} even for the problem of the large deflection dealt with in this study.

The boundary conditions for bending given by Eq. (1) is rewritten in terms of the non-dimensional parameters in the following form.

$$\left.\begin{aligned} &z_n=\pm 1;\ v_n=0 \text{ and } \frac{d^2v_n}{dz_n^2}=0\\ &z_n=0;\ \frac{dv_n}{dz_n}=0 \end{aligned}\right\} \quad \cdots\cdots (36)$$

From Eqs. (35) and (36), Eqs. (32) and (33) yield

$$\frac{dv_n}{dz_n}=-3\int_0^{z_n}\phi_{xn}\,dz_n \quad \cdots\cdots (37)$$

$$v_n=3\int_{z_n}^1\left(\int_0^{z_n}\phi_{xn}\,dz_n\right)dz_n \quad \cdots\cdots (38)$$

$$\delta_n=3\int_0^1\left(\int_0^{z_n}\phi_{xn}\,dz_n\right)dz_n \quad \cdots\cdots (36)$$

Eqs. (34), (35) and (37)$\sim$(39) can be used for the analysis of bending and lateral buckling under monotonic loading. For cyclic loading, increments of the associated parameters are required. They are expressed as

$$\Delta M_{xn}=(1-|z_n|)\,\Delta P_n \qquad \cdots\cdots(40)$$

$$\Delta\phi_{xn}=-\frac{1}{3}\,\Delta\left(\frac{d^2v_n}{dz_n^2}\right) \qquad \cdots\cdots(41)$$

$$\Delta\left(\frac{dv_n}{dz_n}\right)=-3\int_0^{z_n}\Delta\phi_{xn}\,dz_n \qquad \cdots\cdots(42)$$

$$\Delta v_n=3\int_{z_n}^{1}\left(\int_0^{z_n}\Delta\phi_{xn}\,dz_n\right)dz_n \qquad \cdots\cdots(43)$$

$$\Delta\delta_n=3\int_0^{1}\left(\int_0^{z_n}\Delta\phi_{xn}\,dz_n\right)dz_n \qquad \cdots\cdots(44)$$

3.2. Bending under monotonic loading

In order to have a comparison with the results for cyclic loading, the flexural behavior of steel beams under monotonic loading is analyzed. Since the strain distribution is assumed to be symmetrical about the x-axis, it suffices to deal with a half-section of the beam as shown in Fig. 8(a). The section is divided into layers

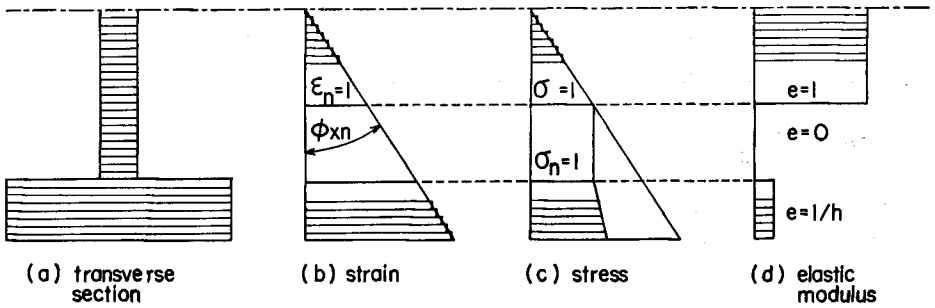

Fig. 8. Laminated Model of Beam and Distribution of Sectional Parameters.

parallel to the x-axis and is analyzed, assuming that the longitudinal strain, stress and tangent modulus, ε_n, σ_n, e, respectively, are constant in each layer, as shown in Fig. 8(b)-(d). In the present analysis, the flange and web of the half section are divided into 25 layers each. To obtain the longitudinal distribution of the required parameters, the half-span length l is divided into 100 uniform intervals.

The numerical procedure consists of (A) obtaining the relation between the curvature ϕ_{xn} and the section parameters including the bending moment M_{xn} and the rigidities $(EI_x)_n$, $(EI_y)_n$, $(EI_w)_n$, and (B) obtaining the distribution of the deformation, rigidities, curvature and bending moment along the length of the beam for a given load. Each stage is described below.

Stage A

(i) Specify the curvature ϕ_{xn}.

(ii) Determine the strain ε_n from Eq. (20).

(iii) Find the stress σ_n and the tangent modulus e from the stress-strain relation in Fig. 5.

(iv) Determine the bending moment M_{xn} from Eq. (18) and the tangent rigidities $(EI_x)_n$, $(EI_y)_n$, and $(EI_w)_n$ from Eqs. (25) and (27).

Stage B

(v) Specify the load P_n.

(vi) Determine the bending moment M_{xn} from Eq. (34) for each section along z-axis.

(vii) From the results of Stage A, find the curvature ϕ_{xn} and the tangent rigidities $(EI_x)_n$, $(EI_y)_n$, $(EI_w)_n$ corresponding to the value of M_{xn} for each section.

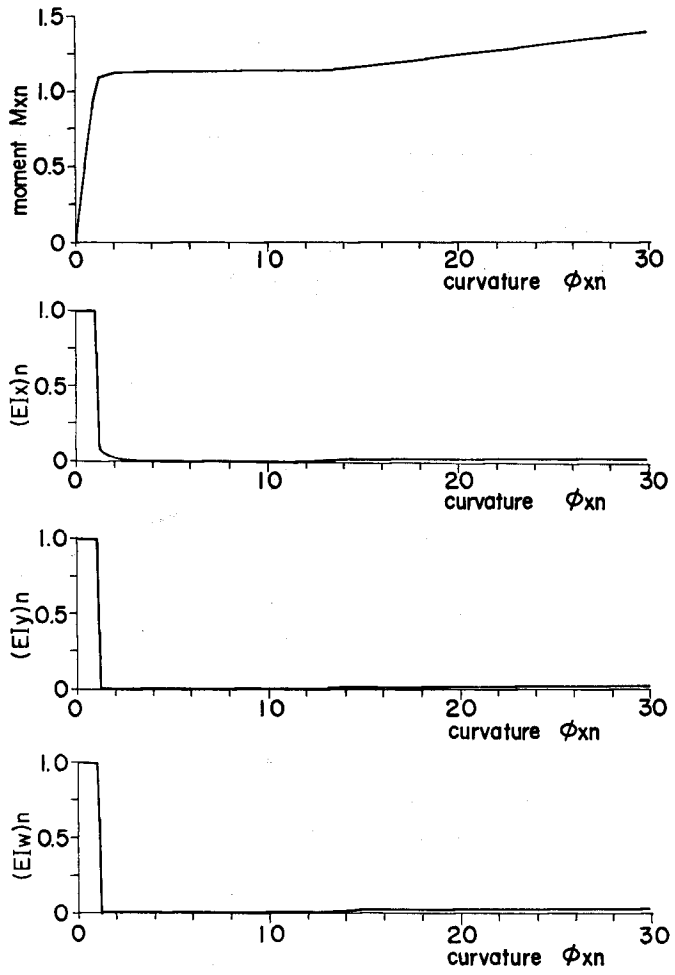

Fig. 9. Bending Moment and Section Rigidities vs. Curvature.

(viii) Find the deflections v_n and δ_n of the beam from Eqs. (37) and (38), respectively.

The rigidities $(EI_y)_n$ and $(EI_w)_n$ obtained above have no relatation to the flexural behavior discussed in this chapter. They are required in the analysis of lateral buckling in the next chapter.

Fig. 9 shows the result of Stage A executed for a steel beam with $100\times100\times6\times8$ mm H-section made of SS41 mild steel whose material properties were described in 2.3. This transverse section gives

$r_x=4.18$ cm, and $r_z=2.47$ cm

In Fig. 9(a), note that the elastic, yielding, and strain-hardening regions are clearly observed. In Fig. 9(b), (c), (d), a rapid loss of the tangent rigidities as the flange yields and a slight recovery in the strain hardening region are observed. Particularly, the flexural rigidity $(EI_y)_n$ and the warping rigidity $(EI_w)_n$ almost vanish in the yield zone since there is little contribution to these two parameters from the web section. This is discussed again in the next chapter in connection with lateral buckling.

Fig. 10 shows the result of Stage B. In Fig. 10, the case where $P_n=1.0$ corresponds to the elastic limit: all parameters in the figure remain in the elastic region. When $P_n=1.15$, the flanges have entirely yielded within the section $|z_n|<0.05$, where the curvature assumes a great value as a result of the loss of rigidity. The loss of rigidity is also observed in $(EI_y)_n$ and $(EI_w)_n$. When $P_n=1.30$, an extended plastic region is observed, and the values of the curvature ϕ_{xn} are great in this extended region, resulting

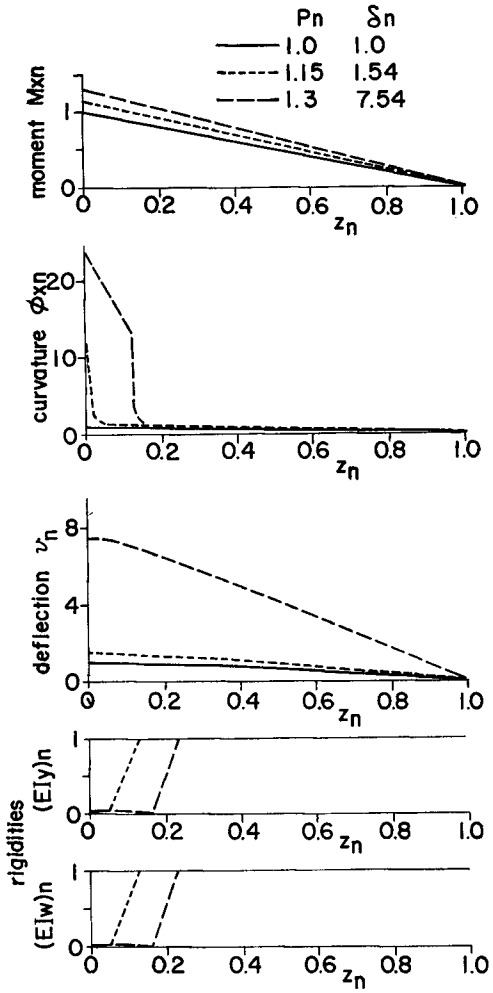

Fig. 10. Longitudinal Distribution of Sectional Parameters under Monotonic Loading.

in a large deflection.

In Fig. 11, the computed $P_n-\delta_n$ relation is compared with a test result[3] for a steel beam with the same section and a half-span length of $l=70$ cm for which the slenderness ratio is $\lambda=70/2.47=28.3$. The computed and test results agree satis-

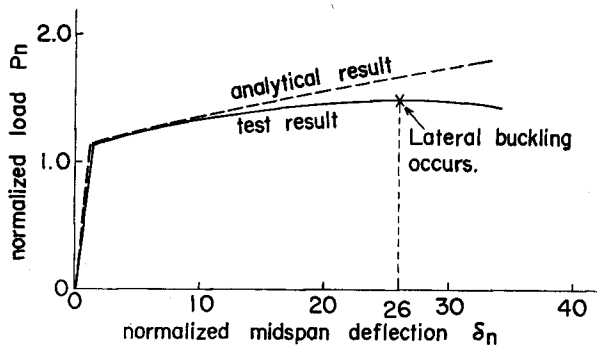

Fig. 11. Load-Deflection Relation under Monotonic Loading.

factorily for $\delta_n<10$ which is a range of practical interest. For greater values of δ_n, however, there is a limit to the value of the load P_n, whereas the computed result increases linearly with δ_n. One reason for this difference can be found in the modeling of the stress-strain relation by a straight line for the strain-hardening region in Fig. 6, that will overestimate the load P_n for a higher region of δ_n. Another and primary reason for a decrease in P_n for higher values of δ_n is the lateral buckling of the tested beam. As the transverse deflection due to lateral buckling grows, the value of P_n attains its maximum value, at $\delta_n=26$ in this case, and decreases for larger values of δ_n.

3.3. Bending under cyclic loading

3.3.1. Procedure of Computation

When the load P_n is cyclic, the moment-curvature relation cannot be definitely determined. This requires a step-by-step analysis for the incremental load ΔP_n in which Stages A and B in the previous section are interrelated. The beam is divided into elements arranged along the y_n- and z_n-axes in the same way as in the case of monotonic loading. Then the numerical procedure for bending under the m-th step of a cyclic loading can be described by the following iterative routine. Let the subscript, m represent the m-th step. The values of $P_{n,m-1}$, $\delta_{n,m-1}$, $v_{n,m-1}$, $M_{xn,m-1}$ and $\phi_{xn,m-1}$ for each section, and $\varepsilon_{n,m-1}$ and $\sigma_{n,m-1}$ for each element must be known.

(i) Specify the load increment $\Delta P_{n,m}$.

(ii) Determine the bending moment increment $\Delta M_{xn,m}$ from Eq. (40) for

each section along the z_n-axis.

(iii) Let $\Delta\phi^{(1)}_{xn,m}=\Delta M_{xn,m}/(EI_x)_{n,m-1}$ be the initial assumed value of iteration for the curvature increment $\Delta\phi_{xn,m}$ corresponding to $\Delta M_{xn,m}$.

(iv) Determine the strain increment $\Delta\varepsilon^{(1)}_{n,m}$ for each element of a section from Eq. (21).

(v) Find the stress increment $\Delta\sigma^{(1)}_{n,m}$ and the tangent modulus $e^{(1)}_{,m}$ for each element from Fig. 5.

(vi) Determine the bending moment increment $\Delta M^{(1)}_{xn,m}$ corresponding to $\Delta\sigma^{(1)}_{n,m}$ from Eq. (22). Determine also the tangent rigidities $(EI_x)^{(1)}_{n,m}$, $(EI_y)^{(1)}_{n,m}$, $(EI_w)^{(1)}_{n,m}$ from Eqs. (25) and (27).

(vii) If $\Delta M^{(1)}_{xn,m}$ is close enough to $\Delta M_{xn,m}$, proceed to (viii). If not, compute $\Delta\phi^{(2)}_{xn,m}=\Delta\phi^{(1)}_{xn,m}+(\Delta M_{xn,m}-\Delta M^{(1)}_{xn,m})/(EI_x)^{(1)}_{n,m}$. Let $\Delta\phi^{(2)}_{xn,m}$ be the second assumed value and return to (iv).

(viii) Complete (ii)$\sim$(vii) for all sections.

(ix) Determine the deflection increments $\Delta v_{n,m}$ and $\Delta\delta_{n,m}$ from Eqs. (43) and (44).

(x) Determine $P_{n,m}$, $\delta_{n,m}$, $M_{xn,m}$ and $\phi_{xn,m}$ for each section, and $\varepsilon_{n,m}$ and $\sigma_{n,m}$ for each element by adding the respective incremental values obtained above to the result of $(m\text{-}1)$-th step.

When the analysis is made for prescribed load steps, it suffices to repeat the above procedure. However, when the loading process is controlled by the deflection amplitude, the deflection $\delta_{n,m}$ obtained in (x) must be checked if it exceeds the prescribed peak value. Suppose that the computation is being made along the route $-①\rightarrow+②$ in Fig. 12. Then for deflection control, the following additional adjustments are necessary.

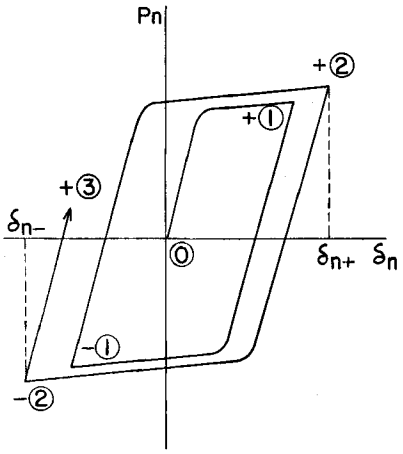

Fig. 12. Illustration of Hysteresis Loop Control.

(xi) If the mid-span deflection $\delta_{n,m}$ obtained in (x) is less than the target peak value δ_{n+}, then return to (i) for the next load step. If $\delta_{n,m}$ exceeds δ_{n+}, proceed to (xii).

(xii) Adjust $\Delta P_{n,m}$ iteratively until the resulting $\delta_{n,m}$ becomes close enough to δ_{n+}, and return to (i) for the next load step on the route $+②\rightarrow-②$ in Fig. 12.

When the m-th step is on the route $+②\rightarrow-②$, the above check is made in a

similar manner. It suffices to replace δ_{n+} and $+②\rightarrow-②$ in the statements of (xi) and (xii) by δ_{n-} and $-②\rightarrow+③$, respectively.

In Figs. 13 and 14, the numerical results obtained from the above procedure for steel beams are compared with the test results. The beams dealt with are again SS41 mild steel 100×100×6×8 mm H-sectioned beams of 70 cm half-span. The test results have been obtained from the preliminary tests or the first few cycles of fatigue tests performed for a previous study[3]. In these figures, the experimental curves are smoother than the analytical curves at the yielding corners except for the initial yielding. This is a consequence of the stress-strain relation model in Fig. 5 which neglects the Bauschinger effect. Therefore, the difference between the analytical and experimental results can be reduced through a refinement of the stress-strain

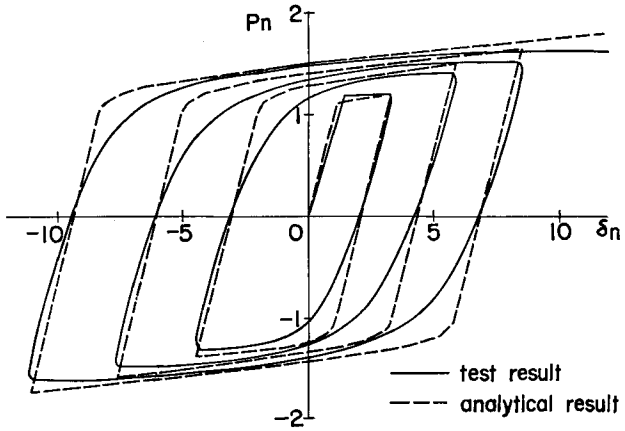

Fig. 13. Transient Hysteresis Curve with Increasing Deflection Amplitude.

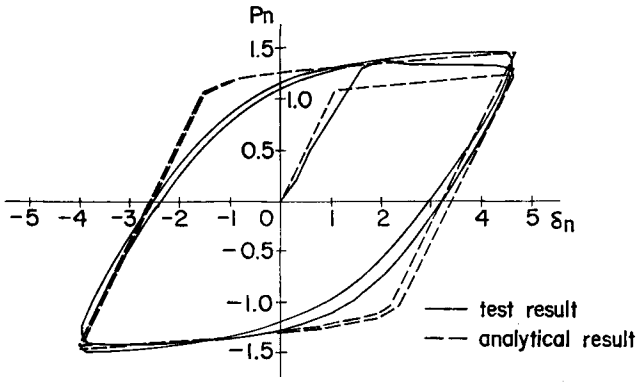

Fig. 14. Transient Hysteresis Curve with Constant Deflection Amplitude (δ_a=4.76).

model, for example, by employing a tri-linear model for repeated hysteretic cycles instead of the bilinear model in Fig. 5. Such a difference will give different results for the hysteretic energy dissipation capacity.

For other aspects of the flexural behavior, however, the analytical and experimental results in Figs. 13 and 14 agree fairly well. In Fig. 13 which corresponds to the increasing deflection amplitude, the analytical result follows the experimental result quite well, particularly in the increase in the load amplitude with an increasing deflection amplitude. In Fig. 14 which is the result for a constant deflection amplitude, the analytical curve again shows a good agreement with the experimental result in that the load amplitude increases with repeated loading cycles which asymptotically attain a stationary state. It should be worth noting that the first and second reverse loading paths ($P_n \rightarrow -P_n$) cross in the negative load region. This is observed for both the analytical and the experimental results. This behavior is discussed in detail in the next subsection. The high initial yield load for the experimental curve in Fig. 14 can be a result of loading frequency of 0.5 Hz.

3.3.2. Tansient Inelastic Flexural Behavior under Constant Deflection Amplitude

First, the transient flexural behavior of inelastic beams is considered. Discussion will be confined to cases for excitation with the constant deflection amplitude of δ_n. Figs. 15 and 16 show the analytical results of the force P_n - displacement δ_n relation for $\delta_a = 4$ and 6, respectively. They can be discussed along with Fig. 14. In Figs. 14~16, it is commonly observed that the absolute value of P_n in the stable hysteresis loops is larger than that for the initial loading path. This is the effect of hardening in the repeated loading cycles, as modeled in Fig. 5. It is also observed that the unloading path in the initial loop (corresponding to $+①\rightarrow -①$ in Fig. 12) crosses with that in the second loop (corresponding to $+②\rightarrow -②$ in Fig. 12), implying that the apparent rigidity for the path $+②\rightarrow -②$ is larger than that for the path $+①\rightarrow -①$. This can be verified from Fig. 17, showing the inelastic regions in each step of loading for $\delta_a=4$.

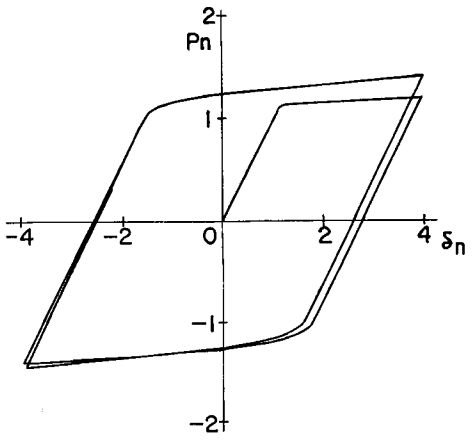

Fig. 15. Transient Hysteresis Curve with Constant Deflection Amplitude ($\delta_a=4$).

Fig. 17(a) corresponds to the step $+①$ at which the inelastic region has not yet fully grown. Most of the inelastic region is in the yield zone. The inelastic

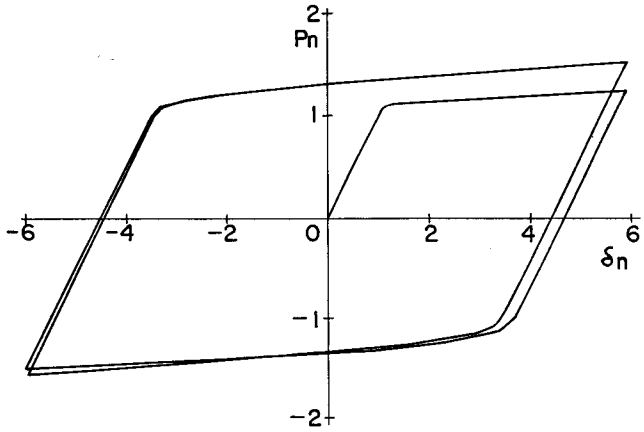

Fig. 16. Transient Hysteresis Curve with Constant Deflection Amplitude ($\delta_a=6$).

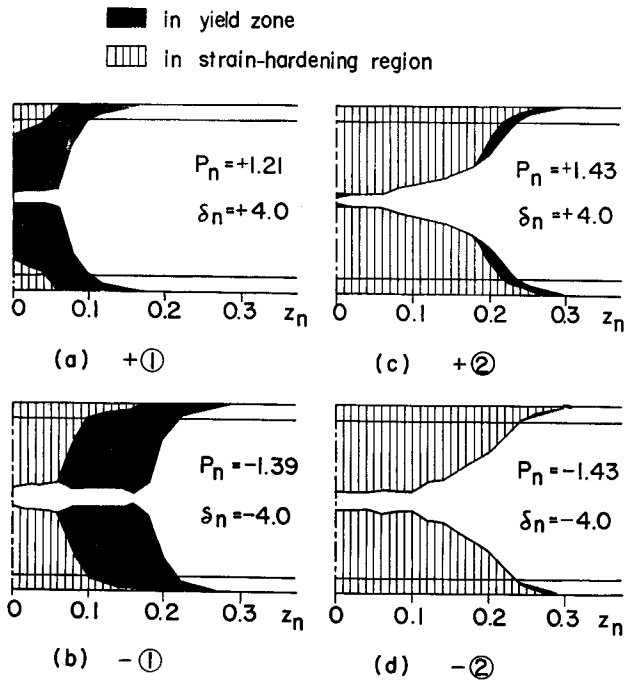

Fig. 17. States of Midspan Plastic Hinge.

region expands on the path +①→−①. The region which yielded before the step +① no longer undergoes the yield zone and is in the strain hardening region at the step −① in Fig. 17(b). However, the region which yielded newly on the path +①→−① is still in the yield zone. On the path −①→+②, only a small region

enters the yield zone, and most of the inelastic region at the step +② in Fig. 17. (c) is in the strain hardening region. Thus, the path +②→−② almost coincides with the steady-state hysteresis loop, resulting in the stable plastic hinge at the step −② as shown in Fig. 17(d). Since almost no yield zone is contained on the path +②→−②, the apparent rigidity is larger than that for the path +①→−① as described above.

The longitudinal distribution of the bending moment, curvature, deflection, and section rigidities are shown in Fig. 18. It may be observed that the curvature at

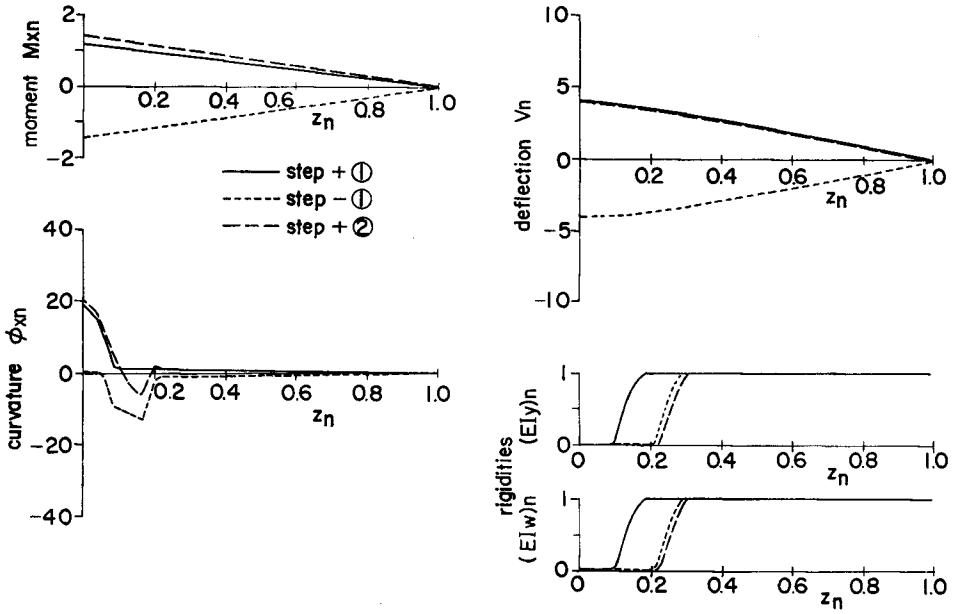

Fig. 18. Longitudinal Distribution of Sectional Parameters under Cyclic Loading ($\delta_a=4$).

midspan for the initial loading step +① affects the curvature distribution at the following steps. As a result, the curvature distribution in the opposite positions of the stationary hysteresis loop (−① and +② in Fig. 18) is not symmeteric. This is also reflected in the configuration of the beam represented by the deflection v_n in Fig. 18. The reduction of the tangent moduli $(EI_y)_n$ and $(EI_w)_n$ in the mid-span region is remarkable. The expansion of the low rigidity region with the loading step is consistent with that of the inelastic region which was discussed above in connection with Fig. 17. Note also that the low rigidity region due to yielding extends more than 20 % of the span, whereas at the initial loading step +① the extension is only 10 %. This difference causes a low deformation capacity against lateral buckling under cyclic loads which will be discussed in the next chapter.

3. 3. 3. Steady-State Inelastic Flexural Behavior under Constant Deflection Amplitude

As shown in the previous subsection, the transient state of the flexural beams treated herein terminates within a few cycles of loading, and a steady-state hysteresis loop is attained. The flexural behavior of the beam under steady-state hysteresis can be analyzed in a simpler manner than the transient case.

In Fig. 18, it was demonstrated that the center of fluctuation of the curvature is shifted toward the side corresponding to the yielding in the initial loading. Therefore, the load amplitudes in the positive and negative loadings do not coincide. However, their difference is within 1 %, and can be neglected. This leads to an assumption that under steady-state hysteresis loops the stress-strain relation also has a stable hysteresis loop in which the stress amplitude σ_a with the positive and negative signs are equal as illustrated by Fig. 19. If the corresponding strain range is denoted by $2\varepsilon_a$, Eq. (8) will hold for all yielded elements.

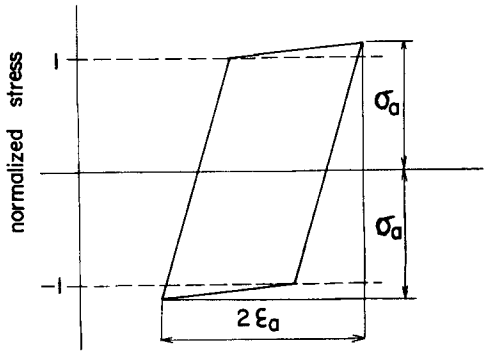

Fig. 19. General Steady-State Stress-Strain Relation.

When both yielded and unyielded elements exist in a cross section, the stress of the unyielded elements is biased, and it is interrelated with the stress of the yielded elements. This situation exists for each yielded section and lasts through the steady-state deformation as shown in Fig. 17(d). A precise description of this state requires the transient analysis described in 3. 3. 2. However, for the analysis of steady-state hysteretic behavior, it will suffice to assume that Eq. (8) holds throughout a section with yielded flanges, since the contribution from the web behavior will be small. Therefore in the present steady-state analysis, it is assumed that Eq. (8) is applicable to each cross section whose flanges have completely yielded. All other sections are treated as elastic.

Then the relation between the load amplitude P_a and the deflection amplitude δ_a at midspan can be obtained in a manner similar to the case of monotonic loading described in 3. 2. The procedure is also divided into two stages as follows.

Stage A

(i) Specify the curvature amplitude ϕ_a.

(ii) Substitute ϕ_a into ϕ_{xn} in Eq. (20). The resulting value of ε_n is the strain amplitude ε_a.

(iii) Find the stress amplitude σ_a using Fig. 19 or Eq. (8). Determine the

tangent modulus $e=1$ or $1/h$ corresponding, respectively, to $\varepsilon_a<1$ and $\varepsilon_a \geqq 1$.

(iv) Substitute σ_a into σ_n in Eq. (18). The resulting value of M_{xn} is the bending moment amplitude M_a. Determine also the tangent rigidities $(EI_x)_a$, $(EI_y)_a$, and $(EI_w)_a$ at $M_{xn}=M_a$ from Eqs. (25) and (27).

Stage B

(v) Specify the load amplitude P_a.

(vi) Substitute P_a into P_n in Eq. (34). The resulting value of M_{xn} is the bending moment amplitude M_a. Repeat this for each section along the z_n-axis.

(vii) From the results of Stage A, find the curvature amplitude ϕ_a and the tangent rigidities $(EI_x)_a$, $(EI_y)_a$, $(EI_w)_a$ corresponding to M_a for each section.

(viii) Substitute ϕ_a into ϕ_{xn} in Eq. (39). The resulting value of δ_n is the mid-span deflection amplitude δ_a.

A numerical result of the above procedure is shown in Fig. 20 along with the result of monotonic loading in Fig. 11. Observe that the load amplitude P_a in cyclic loading assumes a larger value than the load P_n corresponding to the same deflection in monotonic loading. This is a consequence of the absense of yield zones after repetition of loading and also the effect of hardening under repeated loads.

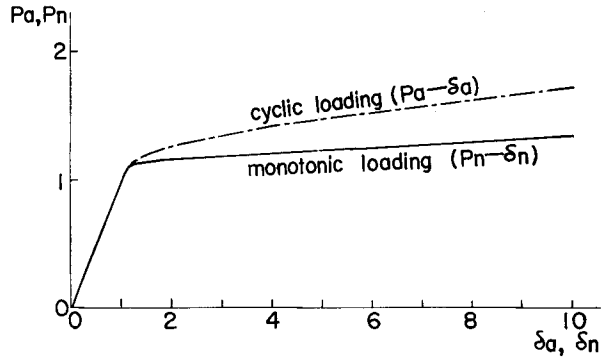

Fig. 20. Load-Deflection Relation.

4. Lateral Buckling of Inelastic Beamds

4.1. Basic analysis

Inelastic buckling of beams under moment gradient generally requires an analysis for variable cross-sections. However, under the basic assumptions employed in 2.4, the stress distribution over a cross-section is symmeteric about the x-axis, so that

the shear center coincides with the centroid. Therefore, $(EI_y)_T$ and $(EI_w)_T$ are the only section parameters that vary along the z-axis. The boundary conditions considered herein which allow no eccentricity of load also simplify the problem.

A somewhat general form of the differential equilibrium equations of the minor axis bending and torsion for a beam in lateral buckling are presented elsewhere[4),9)]. Modifying them to be consistent with the basic assumptions employed in this study yields

$$\left.\begin{aligned}&(EI_y)_T\frac{d^2u}{dz^2}=-\frac{P}{2}(l-z)\,\phi\\&(GJ)_T\frac{d\phi}{dz}-\frac{d}{dz}\left\{(EI_w)_T\frac{d^2\phi}{dz^2}\right\}=\frac{P}{2}(l-z)\frac{du}{dz}-\frac{P}{2}(u_0-u)\end{aligned}\right\}\quad\cdots\cdots(45)$$

for $0\leqq z\leqq l$

in which u_0 is the mid-span lateral deflection which vanishes in this study.

By using the non-dimensional parameters defined so far and introducing some additional parameters, the non-dimensional representation of Eq. (45) becomes

$$\left.\begin{aligned}&(EI_y)_n\frac{d^2u_n}{dz_n^2}=-P_n(1-z_n)\,\phi\\&\alpha\,(GJ)_n\frac{d\phi}{dz_n}-\beta\frac{d}{dz_n}\left\{(EI_w)_n\frac{d^2\phi}{dz_n^2}\right\}=P_n(1-z_n)\frac{du_n}{dz_n}-P_n(u_{on}-u_n)\end{aligned}\right\}\quad\cdots\cdots(46)$$

for $0\leqq z_n\leqq 1$, where

$$u_n=\frac{u}{3\left(\frac{r_x}{r_y}\right)^2\delta_y}\quad\cdots\cdots(47)$$

$$\alpha=a\left(\frac{1}{\varepsilon_Y}\right)^2\left(\frac{1}{\lambda}\right)^2\quad\cdots\cdots(48)$$

$$\beta=b\left(\frac{1}{\varepsilon_Y}\right)^2\left(\frac{1}{\lambda}\right)^4\quad\cdots\cdots(49)$$

$$a=\frac{1}{4}\frac{H^2r_y^2}{r_x^4}\frac{(GJ)_B}{(EI_y)_B}\quad\cdots\cdots(50)$$

$$b=\frac{1}{4}\frac{H^2}{r_x^4}\frac{(EI_w)_B}{(EI_y)_B}\quad\cdots\cdots(51)$$

Considering the anti-symmetry of the mode of buckling dealt with herein, Fig. 1(a), the work done by the external load and the energy stored in the beam are equated in the following form.

$$P_n^2\int_0^1\frac{1}{(EI_y)_n}(1-z_n)^2\phi^2\,dz_n=\alpha\int_0^1(GJ)_n\left(\frac{d\phi}{dz_n}\right)^2dz_n+\beta\int_0^1(EI_w)_n\left(\frac{d^2\phi}{dz_n^2}\right)^2dz_n\quad\cdots\cdots(52)$$

From Eq. (52), it is observed that the buckling load P_b is affected by the coefficients α and β, the tangent rigidities $(GJ)_n$ and $(EI_w)_n$, and the buckling mode ϕ. The basic parameters affecting these quantities are the weak-axis slenderness ratio λ, the yield strain ε_Y, the strain range of the yield zone ε_p, the strain hardening factor h, and the shape of the cross section characterized by a and b.

The Rayleigh-Ritz method is used for obtaining the buckling load P_b. Sine functions are employed as the deformation function satisfying the given boundary conditions. It is given by the following form.

$$\phi=\sum_{i=1}^{m}\phi_i \sin i\pi z_n \qquad \cdots\cdots\cdots (53)$$

in which m is the number of series terms and ϕ_i $(i=1, \ldots, m)$ is the undetermined coefficient for the i-th series term.

Substitution of Eq. (53) into Eq. (52) yields

$$P_n^2\sum_{i,j=1}^{m}A_{ij}\phi_i\phi_j=\sum_{i,j=1}^{m}B_{ij}\phi_i\phi_j \qquad \cdots\cdots\cdots (54)$$

where

$$A_{ij}=\int_0^1\left[\frac{1}{(EI_y)_n}(1-z_n)^2\sin i\pi z_n\sin j\pi z_n\right]dz_n \qquad \cdots\cdots\cdots (55)$$

$$B_{ij}=\int_0^1\left[ij\pi^2\alpha(GJ)_n\cos i\pi z_n\cos j\pi z_n+i^2j^2\pi^4\beta(EI_w)_n\sin i\pi z_n\sin j\pi z_n\right]dz_n \qquad \cdots\cdots\cdots (56)$$

Buckling takes place at the minimum load satisfying Eq. (54) with $\{\phi_i\}\neq\{0\}$; i. e.,

$$\frac{\partial(P_n)^2}{\partial\phi_1}=\frac{\partial(P_n)^2}{\partial\phi_2}=\cdots\cdots=\frac{\partial(P_n)^2}{\partial\phi_m}=0 \qquad \cdots\cdots\cdots (57)$$

which yields

$$\{[B_{ij}]-P_b^2[A_{ij}]\}\{\phi_i\}=\{0\} \qquad \cdots\cdots\cdots (58)$$

Therefore, the buckling load P_b is obtained as the minimum eigenvalue statisfying

$$\det|[B_{ij}]-P_b^2[A_{ij}]|=0 \qquad \cdots\cdots\cdots (59)$$

The procedure for determining P_b is as follows. For a given value of λ, the parameters α and β are determined from Eqs. (48) and (49). Depending on the loading condition specified in terms of P_n or P_a, that is monotonic, transient cyclic, or steady-state cyclic, the tangent rigidities $(EI_y)_n$ and $(EI_w)_n$ are obtained from the procedures described in 3. 2, 3. 3. 1, and 3. 3. 3, respectively. Then all the constants appearing in Eq. (59) are determined from Eqs. (55) and (56), enabling one to obtain the value for P_b.

The critical load P_{cr} at which the lateral buckling actually occurs is obtained as the value of P_b when $P_b=P_n$. Let δ_{cr} be the value of the mid-span deflection δ_n corresponding to P_{cr}. Then δ_{cr} may be referred to as the deformation capacity of the beam against lateral buckling. This is illustrated in Fig. 21 which is a case for

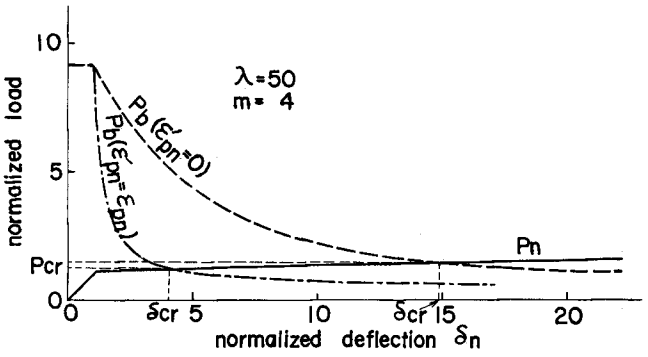

Fig. 21. Lateral Buckling Load under Monotonic Loadng.

$\lambda=50$, $m=4$. Observe that there is a slight difference in P_{cr} and a great difference in δ_{cr} depending on $\varepsilon'_{pn}=\varepsilon_{pn}$ or 0. This nature is discussed in detail in a later section.

4.2. Convergence of solution

The accuracy of the critical load P_{cr} and the deformation capacity δ_{cr} will depend on the number of terms m in the series in Eq. (53) giving the buckling mode. In the analysis of elastic buckling, convergence of the solution with m is very rapid; error in P_{cr} is of the order of[9] 1% for $m=1$. However, the error for inelastic buckling becomes much worse.

Fig. 22 is a plot of the load P_n and the corresponding buckling load for the various values of m and for $\varepsilon'_{pn}=\varepsilon_{pn}$, Fig. 22(a), and $\varepsilon'_{pn}=0$, Fig. 22(b). Because of the stationary nature of the eigenvalue, P_b decreases with increasing m. It may be observed that P_b depends more on m in the inelastic region ($\delta_n>1$).

Fig. 23 shows the variation of P_{cr} with m for the various values of the weak-axis slenderness ratio λ. For a small value of λ, say $\lambda=50$, the change in P_{cr} with m is great when m is small, whereas it assumes an almost constant value for $m>8$. When λ is large, say $\lambda=200$, P_{cr} varies over a wider range of m. However, the rate of variation is small. Similar statements can be made for the deformation capacity δ_{cr} shown in Fig. 24, although δ_{cr} is more sensitive to m than P_{cr} as implied by Fig. 21. Based on these results it will suffice to take $m=10$. This value is used for the subsequent numerical calculations.

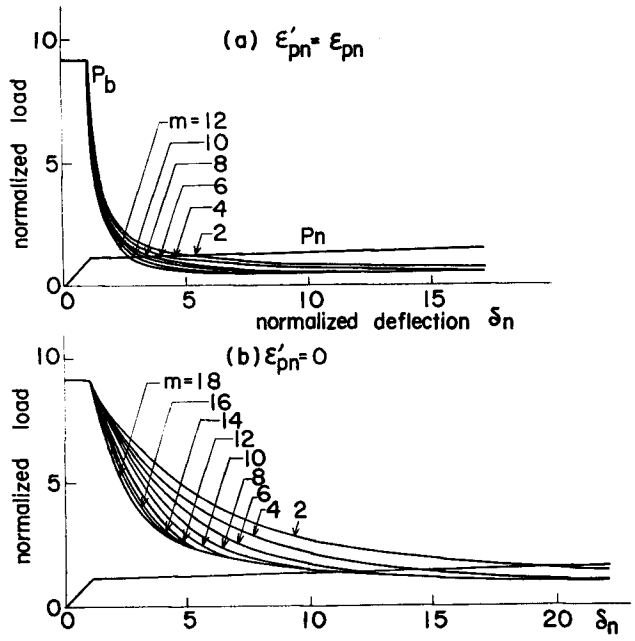

Fig. 22. Lateral Buckling Load under Monotonic Loading ($\lambda=50$).

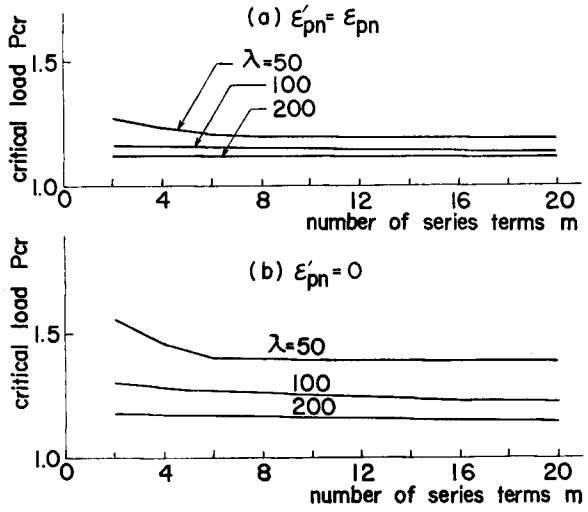

Fig. 23. Convergence of Critical Load.

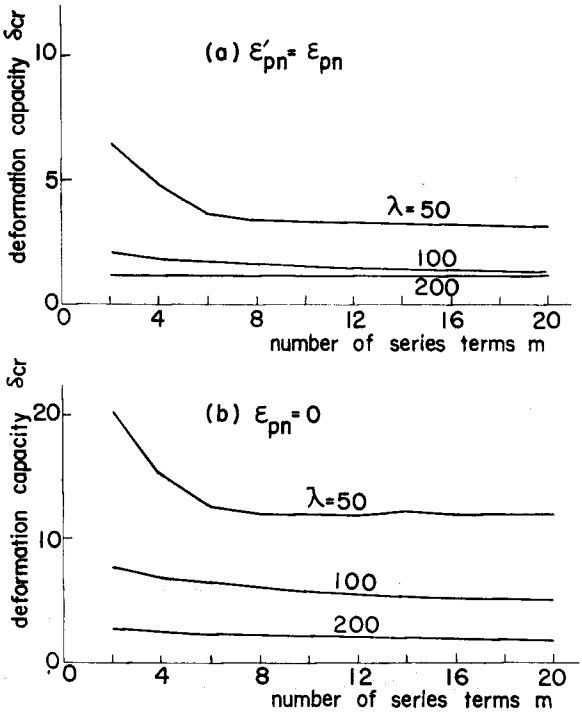

Fig. 24. Convergence of Deformation Capacity.

4.3. Critical load and deformation capacity under various loading patterns

4.3.1. Monotonic Loading

The critical load of a 100×100×6×8 mm H beam made of SS41 mild steel is plotted against the weak-axis slenderness ratio λ in Fig. 25. In the region for $\lambda>310$ only elastic buckling takes place and is not considered in Fig. 25. It may be observed in Fig. 25 that P_{cr} for $\varepsilon'_{pn}=0$ always exceeds that for $\varepsilon'_{pn}=\varepsilon_{pn}$. This difference is great for short beams with a small λ. This tendency is much more remarkable in Fig. 26 which shows the deformation capacity δ_{cr} plotted against λ. Particularly in the range of $\lambda=100\sim280$, δ_{cr} for $\varepsilon'_{pn}=0$ gradually increases with a decrease in λ, whereas δ_{cr} for $\varepsilon'_{pn}=\varepsilon_{pn}$ is almost constant, with values slightly greater than one. In the case of $\varepsilon'_{pn}=\varepsilon_{pn}$, yielding of the flanges result in almost a complete loss of the tangent rigidities $(EI_y)_n$ and $(EI_w)_n$ in the presence of a yield zone that is the reason for a low deformation capacity regardless of the value of λ. In the range of $\lambda<100$, the effect of torsional rigidity becomes dominant and δ_{cr} increases with a decreasing λ for $\varepsilon'_{pn}=\varepsilon_{pn}$ also.

The significance of taking $\varepsilon'_{pn}=\varepsilon_{pn}$ and 0 may be judged by comparing these analytical results with experimental data. In Figs. 27 and 28, part of the extensive

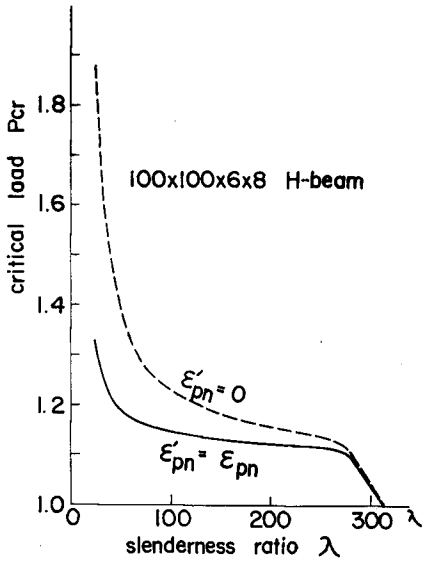

Fig. 25. Critical Load under Monotonic Loading.

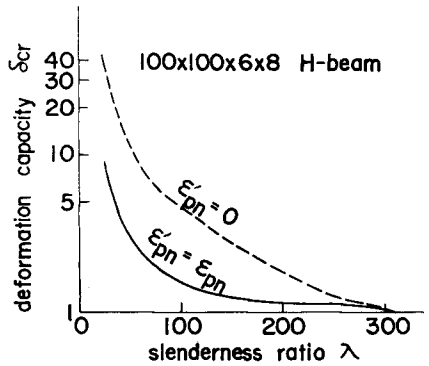

Fig. 26. Deformation Capacity under Monotonic Loading.

experimental data obtained by Udagawa, Saisho, Takanashi and Tanaka[10] is shown along with the analytical results obtained from the method of this study. They are the results for the SS41 H-sectioned ($200\times100\times5.5\times8$ mm) steel beams. Fig. 27 shows the critical load P_{cr}, and Fig. 28 shows the deformation capacity δ_{cr}.

The experimental data marked by $\times$ corresponds to a load level at which a lateral deflection of the flanges is observed. However, this lateral deflection usually does not grow further until the maximum load is attained at which an excessive lateral deflection due to lateral buckling takes place[2] and unloading follows. The data marked by $\bigcirc$ in the figures correspond to the maximum load.

It can be observed that the analytical results for $\varepsilon'_{pn}=\varepsilon_{pn}$ agree fairly well with the experimental data for flange lateral deflection. Although the analytical result for $\varepsilon'_{pn}=0$ lies only between the experimental data for the flange lateral deflection and the maximum load, it may be compared with the data for the maximum load. If the above

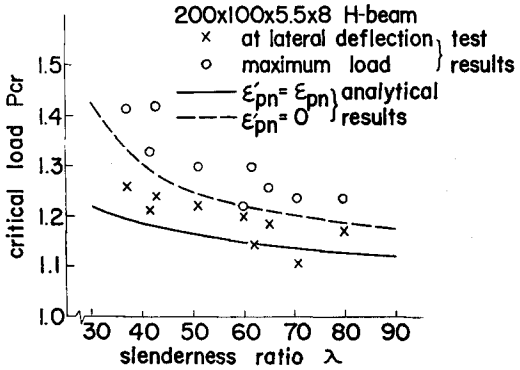

Fig. 27. Critical Load under Monotonic Loading (Test results are after Udagawa et. al.[10]).

comparison is allowed, the following statement may be made in the light of discussion on the basic assumption (vii) in 2.4. The yielding of a whole flange section causes instantaneous loss of the tangent rigidities $(EI_y)_n$ and $(EI_w)_n$ and this initiates a flange deflection due to lateral buckling. This corresponds with the result for $\varepsilon'_{pn}=\varepsilon_{pn}$. However, the yield zone can exist only instantaneously, so that the lateral deflection of flanges does not grow further, and the load and the flexural deflection can increase beyond this limit. The final excessive lateral buckling takes place in the strain hardening region corresponding to $\varepsilon'_{pn}=0$ that gives the maximum load. More detailed comparisons of the numerical values between the analytical results and the experimental data are

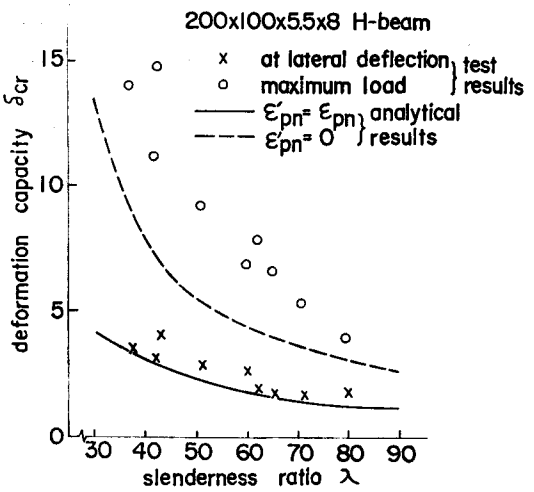

Fig. 28. Deformation Capacity under Monotonic Loading (Test results are after Udagawa et. al.[10]).

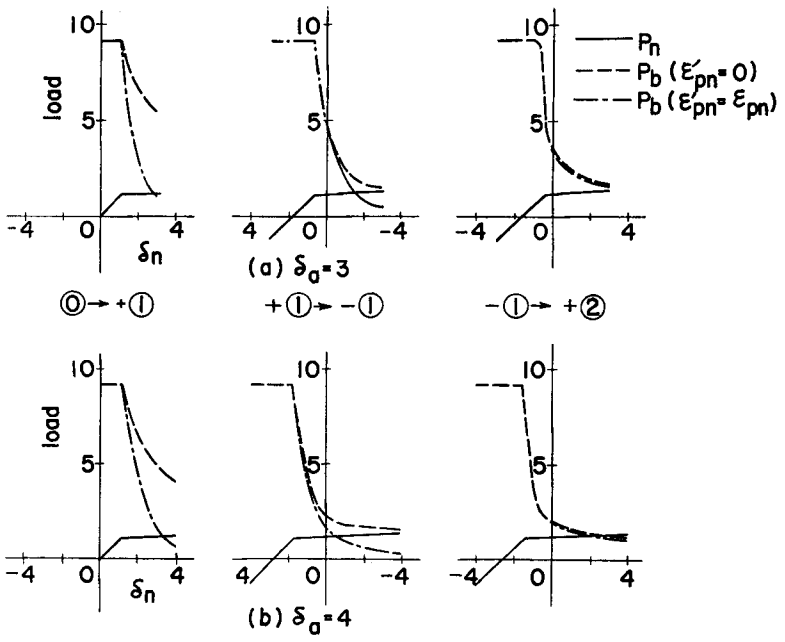

Fig. 29. Buckling Load under Transient Cyclic Loading.

impossible since the actual beams contain irregularities including the residual stress, etc. However, the above statements may be justified qualitatively as major factors affecting the lateral buckling under monotonic loading. Moreover, from the above discussion, the values of P_{cr} and δ_{cr} for $\varepsilon'_{pn}=0$ denoted by $\bar{P}_{cr}$ and $\bar{\delta}_{cr}$, respectively, may by more significant than those for $\varepsilon'_{pn}=\varepsilon_{pn}$ for practical engineering purposes.

4.3.2. Cyclic Loading with Constant Deflection Amplitude—Transient State

When steel beams are subjected to cyclic loading with the constant mid-span deflection amplitude δ_a, there are three possible ways for an occurrence of lateral buckling[2]: (i) a limited lateral deflection due to buckling takes place in the first loading step but does not grow further throughout subsequent cyclic loadings, (ii) similar to the previous case in the first loading step but excessive buckling takes place during a subsequent cyclic loading, and (iii) excessive buckling takes place during the first loading step.

These cases may be explained from the results of analysis using the method of this study. Fig. 29 shows the variation of the buckling load P_b in each transient loading step identified in the same manner as in Fig. 12. These results are for steel beams with a cross-sectional shape similar to those in Figs. 25 and 26, and the weak-axis slenderness ratio of $\lambda=50$. Fig. 29(a) is for a case where the deflection amplitude is $\delta_a=3$. Observe that the buckling load P_b for $\varepsilon'_{pn}=\varepsilon_{pn}$ becomes smaller than the applied load P_n in the loading steps ⓪→+① and +①→−①, whereas the value of P_b for $\varepsilon'_{pn}=0$ exceeds P_n for all the loading steps accounted for in Fig. 29(a). Thus, a lateral buckling with $\varepsilon'_{pn}=\varepsilon_{pn}$ takes place, but, there is no further growing of deformation since a buckling with $\varepsilon'_{pn}=0$ does not occur. Hence, it corresponds to case (i) of the above mentioned three cases.

In Fig. 29(b), which corresponds to a larger deflection amplitude with $\delta_a=4$, it is observed that P_b for $\varepsilon'_{pn}=\varepsilon_{pn}$ becomes smaller than P_n in the loading steps ⓪→+① and +①→−①, and at the same time, the P_b values for $\varepsilon'_{pn}=0$ also become smaller than P_n during subsequent stationary loading cycles. Hence, in this case an excessive lateral buckling takes place and this result will correspond to case (ii). In this case, the practical deformation capacity $\bar{\delta}_{cr}$ is apparently smaller than that for monotonic loading since a buckling with $\varepsilon'_{pn}=0$ does occur for a deflection amplitude δ_a which is much smaller than the $\bar{\delta}_{cr}$ value for monotonic loading.

Case (iii) occurs when P_b for $\varepsilon'_{pn}=0$, as well as that for $\varepsilon'_{pn}=\varepsilon_{pn}$ becomes smaller than P_n before the loading step −①. Up to this step, a clear yield zone exists as shown in Fig. 17. If this takes place before the step +①, the situation is identical with the buckling in monotonic loading discussed in 4.3.1.

4. 3. 3. Cyclic Loading with Constant Deflection Amplitude—Steady State

As shown in the discussion for case (ii) in the previous subsection, the practical deformation capacity against lateral buckling is usually smaller than that for monotonic loading. The main reason for this is an increase in the load level P_n with a repetition of load cycles under the constant deflection amplitude δ_a which was discussed in 3. 3. 2. This nature can be examined by obtaining the relation between $\bar{P}_{cr}$ and $\bar{\delta}_{cr}$ for a steady state flexural behavior and comparing it with the result for monotonic loading.

Fig. 30 shows the critical load $\bar{P}_{cr}$ for cyclic and monotonic loadings. It may be concluded from this result that the critical load for lateral buckling actually does not depend on the loading mode. The question, therefore, is at what value of deflection the load level P_n will reach $\bar{P}_{cr}$ depending on the loading mode.

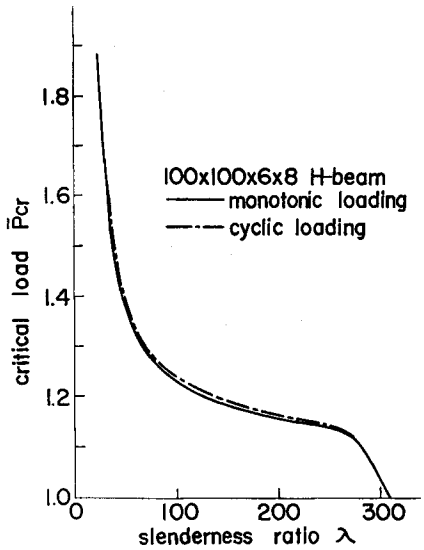

Fig. 30. Practical Critical Load.

Fig. 31 is a plot of the deformation capacity $\bar{\delta}_{cr}$ for cyclic and monotonic loadings. Observe that there is a great difference between the $\bar{\delta}_{cr}$ values for the two loading modes. From these results, it is clear that the increase in the load level P_n caused by the vanishing of the yield zone and the successive hardening during the cyclic flexural deformation results in a small deformation capacity

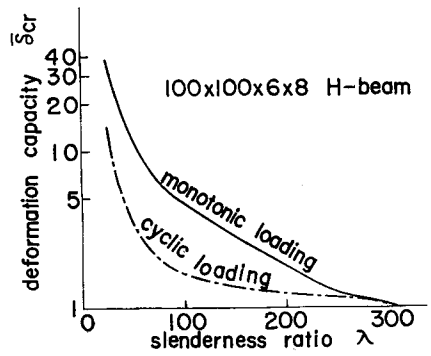

Fig. 31. Practical Deformation Capacity.

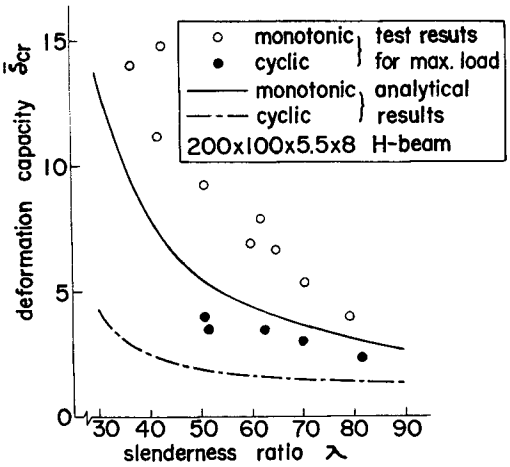

Fig. 32. Practical Deformation Capacity (Test results are after Tanaka et. al.[81]).

under cyclic loading. This is also justified by experimental data obtained by Tanaka et al.[8] as shown in Fig. 32 along with the analytical result of this study.

5. Summary and Conclusions

Flexural behavior and lateral buckling of inelastic mild-steel beams were analyzed in this study. Analytical results were discussed to provide a sound physical basis for interpretation of the phenomena. For this purpose, previous experimental data were also referred to. The major results obtained herein can be summarized as follows.

(1) By using the analytical model proposed in this study, the transient flexural behavior and the lateral buckling of inelastic steel beams can be analyzed with a consideration of the yield zone, strain hardening, and hardening in cyclic load reversals.

(2) The analytical result of load-deflection hysteresis loops obtained from the method of this study permits a physical interpretation of the detailed transient flexural behavior of inelastic mild-steel beams. It is characterized by a low rigidity during the first cycle of loading and a hardening in subsequent load reversals that is a consequence of the vanishing of the yield zone of the plastic hinge and the successive hardening in cyclic loads.

(3) The lateral buckling load P_{cr} of mild-steel beams with an H-section under monotonic loading varies depending on the treatment of yield zone; i. e., (i) the strain range of the yield zone ε_{pn} in flexural analysis is considered also for lateral deflection in buckling, that is $\varepsilon'_{pn}=\varepsilon_{pn}$, or (ii) it is not considered, that is $\varepsilon'_{pn}=0$. From a discussion of the nature of the yield zone and a comparison with experimental data, it may be stated that case (i) occurs during lateral buckling with an instantaneous complete loss of rigidity caused by flange yielding which results in a limited lateral deflection, whereas case (ii) occurs in excessive lateral buckling corresponding to a maximum load carried by the beam that may be taken as the critical load $\bar{P}_{cr}$ for practical purposes.

(4) The same is true of the deformation capacity δ_{cr} for lateral buckling. However, the deformation capacity is more sensitive to the two cases described above than the buckling load.

(5) In lateral buckling under cyclic loads, the question is that case (i) may occur in the first loading step or case (ii) may occur during any loading step. For the practical critical load $\bar{P}_{cr}$, the P_{cr} value for case (ii) may be chosen for cyclic load also.

(6) The practical buckling load $\bar{P}_{cr}$ for monotonic loading and that for cyclic loading are almost indentical, whereas the corresponding deformation capacicy $\bar{\delta}_{cr}$

for cyclic loading is much smaller than that for monotonic loading. This can be explained as a consequence of a hardening of the beam in reversed flexural deformations. This result agrees qualitatively with the experimental data. These results should provide useful information for the design of structural beam members subjected to cyclic deformation during strong earthquakes.

Acknowledgment

This study was motivated by the results of the experimental studies performed at Kyoto University by a research group including some of the authors. Contributions of the members who participated in the series of experiments are gratefully acknowledged. Special thanks are due to Dr. T. Koike, presently with the Kawasaki Steel Corporation, for his contribution to the test project as well as his constructive comments on the present study. The authors are also indebted to other researchers, particularly Professors H. Tanaka, K. Takanashi, and their research group at the University of Tokyo, who have published valuable experimental data which played an important role for comparing the analytical and test results in this study.

Refernces

1) Fujimoto, M., Moriya, K., and Wada, A, "Studies on the Mechanical Properties of Structural Steel and Steel Members," *Transactions*, Architectural Institute of Japan, No. 167, Jan., 1970, pp. 13-24, (in Japanese).
2) Goto, H., Kameda, H., Koike, T., Izunami, R., Wakita, K., and Sugihara, Y., "A Consideration on Failure Process of Structural Steel under Repeated Flexural Loads," *Annuals*, Disaster Prevention Research Institute, Kyoto Univ., No. 17B, Oct., 1974, pp. 157-169, (in Japanese).
3) Goto, H., Kameda, H., Koike, T., Aoyama, I., and Wakita, K., "Probabilistic Considerations on Plastic Fatigue Failure of Structural Steel," *Annuals*, Disaster Prevention Research Institute, Kyoto Univ., No. 18B, April, 1975, pp. 377-393, (in Japanese).
4) Kitipornchai, S., and Trahair, N. S., "Buckling of Inelastic I-Beams under Moment Gradient," *Journal of the Structural Division*, ASCE, Vol. 101, No. ST5, May, 1975, pp. 991-1004.
5) Lay, M. G., "Yielding of Uniformly Loaded Steel Members," *Journal of the Structural Division*, ASCE, Vol. 91, No. ST6, Dec., 1965, pp. 49-66.
6) Takanashi, K., "Inelastic Lateral Buckling of Steel Beams Subjected to Repeated and Reversed Loadings," *Proceedings*, 5th World Conference on Earthquake Engineering, Rome, 1973, Vol. 1, pp. 795-798.
7) Tanabashi, R., Yokoo, Y., Nakamura, T., Kubota, T., and Yamamoto, A., "Load-Deflection Behaviors and Plastic Fatigue of Wide-Flange Beams Subjected to Alternating Plastic Bending," *Transactions*, Architectural Institute of Japan, No. 176, Oct., 1970, pp. 25-35.
8) Tanaka, H. Takanashi, K., and Udagawa, K., "Inelastic Lateral Buckling of Steel Beams Subjected to Repeated and Reversed Loadings," *Seisan-Kenkyu*, Institute of Industrial Science, Univ. of Tokyo, Vol. 25, No. 2, Feb, 1973, pp. 47-52, (in Japanese).
9) Timoschenko, S. P., and Gere, J. M., "Theory of Elastic Stability," 2nd ed., McGraw-Hill, 1961.
10) Udagawa, K., Saisho, M., Takanashi, K., and Tanaka, H., "Experiments on Lateral Buckling of H-Shaped Beams Subjected to Monotonic Loadings," *Transactions*, Architectural Institute of Japan, No. 212, Oct., 1973, pp. 23-33.

11) Vann, W. P., Thompson, L. E., Whalley, L. E., and Ozier, L. E.. "Cyclic Behavior of Rolled Steel Members," *Proceedings*, 5th World Conference on Earthquake Engineering, Rome, 1973, Vol. 1, pp. 1187-1193.
12) Watanabe, H., "Dynamic Characteristics of Elasto-Plastic Restoring Force of Mild Steel," *Proceedings*, JSCE, No. 182, Oct., 1970, pp. 1-18, (in Japanese).

Appendix. Notation

A = area element
A_n = normalized area element
A_o = total sectional area
a = parameter for Eq. (46)
B = width of flange
b = parameter for Eq. (46)
E = elastic modulus
E_h = strain hardening modulus
E' = tangent modulus
e = E'/E = normalized tangent modulus
EI_f = flexural rigidity of a single flange about y-axis
EI_w = warping rigidity
EI_x = strong axis flexural rigidity
EI_y = weak axis flexural rigidity
G = shear modulus
GJ = torsional rigidity
H = height of H-beam
h = E/E_h = strain hardening factor
l = half span length
M_a = bending moment amplitude about x-axis
M_x, M_y = bending moment about x- and y-axes, respectively
M_{xn}, M_{yn} = normalized bending moment about x- and y-axes, respectively
M_{xY} = yield bending moment about x-axis
m = number of series terms in the Rayleigh-Ritz method for lateral buckling
P = external load applied at mid-span
P_a = normalized load amplitude
P_b = buckling load
P_{cr} = critical load for lateral buckling
$\bar{P}_{cr}$ = practical critical load (P_{cr} value for $\varepsilon'_{pn}=0$)
P_n = P/P_Y = normalized load
P_Y = yield load
r_x, r_y = radius of gyration about x- and y-axes, respectively

t_f, t_w = thickness of flange and web, respectively
u, v = deflection in x- and y-directions, respectively
u_n, v_n = normalized deflections
v_Y = deflection at yielding of flanges
x, y, z = position co-ordinates
x_n, y_n, z_n = normalized position co-ordinates
ΔM_{xn}, ΔM_{yn} = normalized bending moment increments
Δv_n = normalized deflection increment
$\Delta \delta_n$ = normalized mid-span deflection increment
$\Delta \varepsilon$ = strain increment
$\Delta \varepsilon_n$ = normalized strain increment
$\Delta \sigma$ = stress increment
$\Delta \sigma_n$ = normalized stress increment
$\Delta \phi_{xn}$ = normalized curvature increment about x-axis
δ_a = normalized mid-span deflection amplitude
δ_{cr} = normalized deformation capacity for lateral buckling
$\bar{\delta}_{cr}$ = normalized practical deformation capacity (δ_{cr} value for $\varepsilon'_{pn}=0$)
δ_n = normalized mid-span deflection
δ_Y = yield deflection
ε = fiber normal strain
ε_a = strain amplitude
ε_n = $\varepsilon/\varepsilon_Y$ = normalized strain
ε_p = strain range of yield zone